

Supplementary information

Supplementary figures

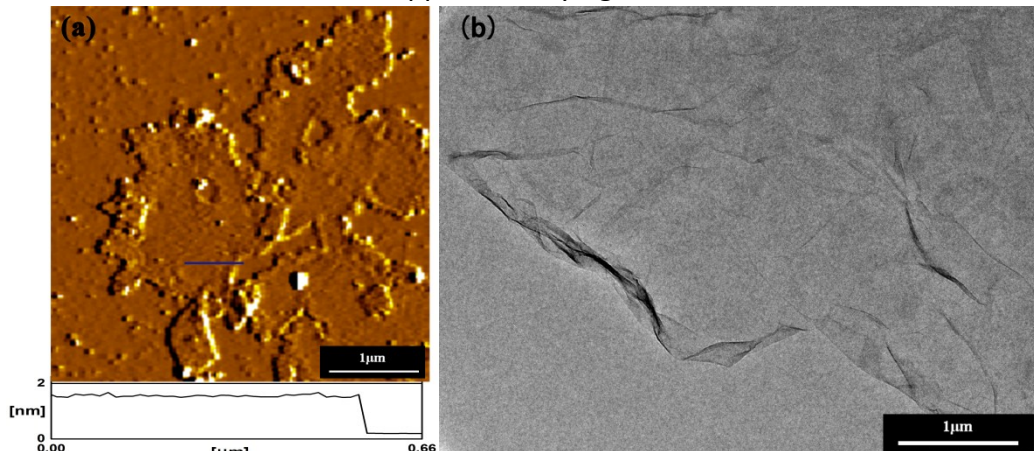


Figure S1 (a) AFM image of graphene oxide, (b) TEM image of graphene oxide

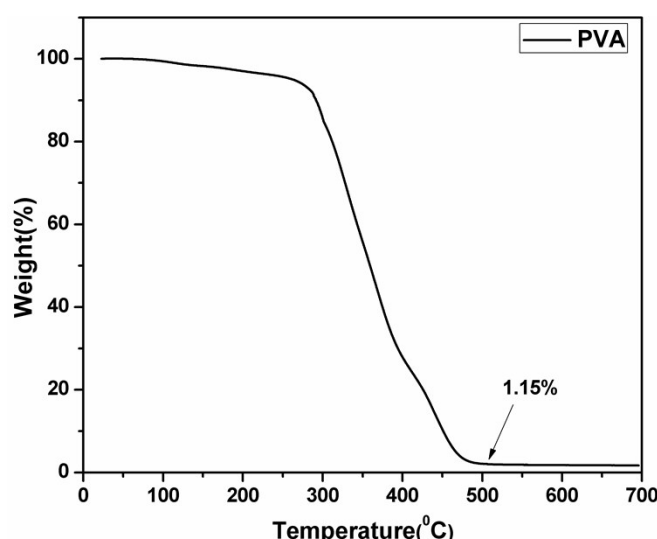


Figure S2. TGA thermograms of PVA under nitrogen

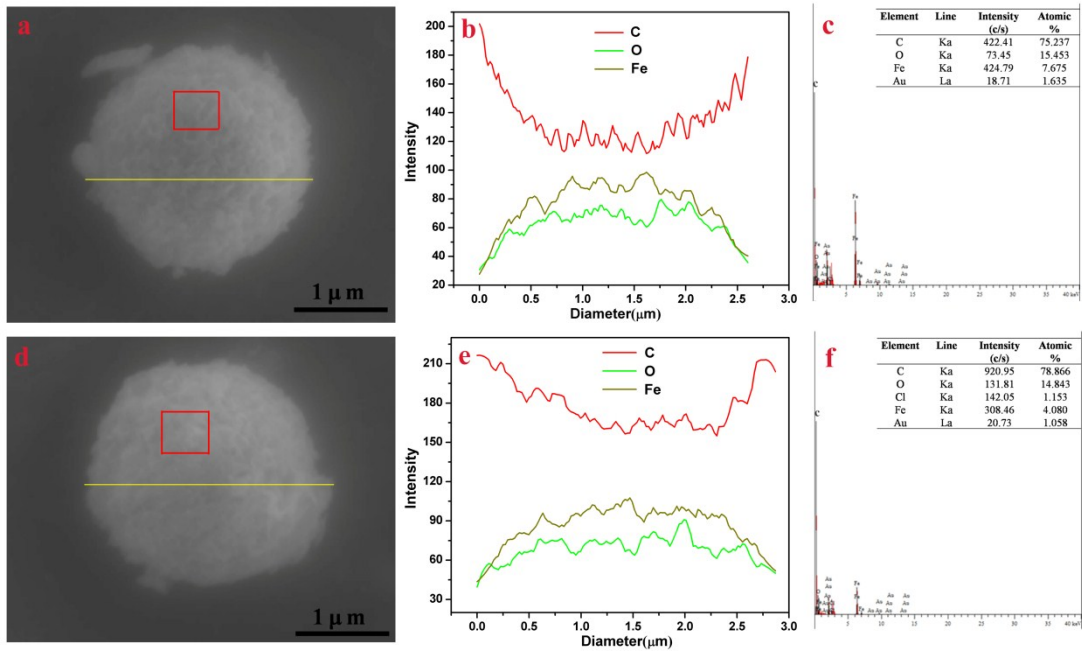


Figure S3 (a)SEM of a single Air@rGO@Fe₃O₄ microsphere; (b) Line scanning profiles of different elements recorded along the yellow line shown in panel (a); (c) EDS spectrum of the red area shown in panel (a); (d) SEM of a single Air@rGO@Fe₃O₄ microspheres soaked in hydrochloric acid solution 5 days; (e) Line scanning profiles of different elements recorded along the yellow line shown in panel (d); (f) EDS spectrum of the red area shown in panel (d).

Supplementary notes

Supplementary Note 1: Microwave absorption measurements

The reflection loss (RL) was calculated based on the relative complex permittivity and permeability at a given frequency and thickness according to the following equations:¹

$$Z_{in} = \sqrt{\mu_r / \epsilon_r} \tanh \left[-j(2\pi f d / c) \sqrt{\mu_r / \epsilon_r} \right] \quad (1)$$

$$RL(\text{dB}) = 20 \log_{10} |(Z_{in} - 1) / (Z_{in} + 1)| \quad (2)$$

where ϵ_r and μ_r are the relative complex permittivity ($\epsilon_r = \epsilon' - j\epsilon''$) and permeability ($\mu_r = \mu' - j\mu''$) of the absorber, f is the frequency of microwave in free space, c is the velocity of light, d is the coating thickness and Z_{in} is the input impedance of the absorber.

Supplementary Note 2: Basic concepts and the dielectric loss mechanism of Air@rGO@Fe₃O₄ microspheres

Debye dipolar relaxation is an important mechanism for the dielectric loss of microwave absorbing materials and can be confirmed by Cole-Cole plots. Based on the Debye dipolar relaxation expression, the relationship between ϵ' and ϵ'' can be deduced and expressed by the following equation:²

$$\left(\epsilon' - \frac{\epsilon_s + \epsilon_\infty}{2} \right)^2 + (\epsilon'')^2 = \left(\frac{\epsilon_s - \epsilon_\infty}{2} \right)^2 \quad (3)$$

Where ϵ_s and ϵ_∞ are the static permittivity and relative dielectric permittivity at the high-frequency limit, respectively. It is easy to see that the plot of ϵ' versus ϵ'' would be a single semicircle, generally regarded as the

Cole–Cole semicircle. Each semicircle corresponds to one Debye relaxation process. In the present work, four semicircles were found from the curve of the Air@rGO@Fe₃O₄ in Fig. 8d. The presence of one standard semicircle, which was depicted based on the dielectric data obtained from the range of 1–8.5GHz, suggests that Debye dipolar relaxation is main dielectric loss mechanism in this frequency domain. The other nonstandard or distorted semicircles indicate other mechanisms such as the Maxwell–Wagner relaxation, electron/ion polarization and dipolar polarization, also exist in addition to the Debye relaxation.^{3–6} By contrast, Cole-Cole plots of rGO nanosheets or Fe₃O₄ nanoparticles show there are several weaker or no Debye relaxation process, respectively. As is known, Debye relaxation process is helpful for the enhancement of dielectric properties. Therefore the fourfold dielectric relaxation processes suggest that the Air@rGO@Fe₃O₄ facilitate multiple dielectric losses, resulting in enhancement of microwave absorbing properties.

Supplementary Note 3: Basic concepts and the magnetic loss mechanism of Air@rGO@Fe₃O₄ microspheres

In general, magnetic loss mechanism of magnetic materials includes hysteresis loss, eddy current loss and residual loss, such as domain resonance, natural resonance, and exchange resonance. The magnetic hysteresis loss is exclusively generated from irreversible magnetization in a strong applied field. The domain wall resonance for the multidomain Fe₃O₄ materials only occurs in the frequency region below 2GHz, whereas the magnetic loss mechanism for the single-domain Fe₃O₄ in the frequency region of 2–18GHz mainly originates from natural resonance, exchange resonance, and eddy current loss. In present work, it can be observed from Fig. 8e-f that there are several multiresonance peaks in the μ' and μ'' curves for Air@rGO@Fe₃O₄ microspheres and Fe₃O₄ nanoparticles. The peaks detected at the low-frequency range of 2–6GHz are related to natural resonance, and the difference in the shape and shift of two natural resonance peaks can be attributed to either the small size effect or high shape anisotropy.⁷ These observed middle-frequency (6–12GHz) resonance peaks belong to exchange resonances, which are generally related to polarizable Fe²⁺ ions in the spinel structure, vacancy and space-charge polarization, or surface effect and spin wave excitations.^{3, 8, 9}

Under an alternating magnetic field, the conductive materials can generate the eddy current due to electromagnetic induction. The eddy current effect can attenuate incident electromagnetic wave, whereas it also prevents a large part of electromagnetic waves from entering the inner of absorber agent. According to skin-effect criterion, the eddy-current loss can be evaluated by the following equation:¹⁰

$$\mu''(\mu'^{-2}f^{-1}) = 2\pi\mu_0\sigma d^2/3 \quad (4)$$

Where μ_0 is the vacuum permeability, σ is the electronic conductivity and d is the sample thickness. If magnetic loss resonance peak solely originates from eddy current loss effect, the values of $\mu''(\mu'^{-2}f^{-1})$ will keep constant with changing f . As seen from Fig. 8h, these values are almost unchanged for Fe₃O₄ nanoparticles over 12–18GHz, indicating that magnetic loss is mainly caused by eddy current effect. The similar results were found when investigate Fe₃O₄ nano particles². However, the curve of Air@rGO@Fe₃O₄ microspheres shows a significant fluctuation in this frequency range, and thus the eddy current can be rule out. The lack of eddy current may perform a crucial function in the enhancement of electromagnetic absorption properties for Air@rGO@Fe₃O₄ microspheres.

Supplementary Note 4: Basic concepts of impedance matching ratio and attenuation constant

The enhanced microwave absorption properties mainly resulted from the impedance matching Z and attenuation constant α , as expressed by the following equation:^{10, 11}

$$\alpha = \frac{\sqrt{2\pi f}}{c} \times \sqrt{(\mu''\epsilon'' - \mu'\epsilon') + \sqrt{(\mu''\epsilon'' - \mu'\epsilon')^2 + (\mu'\epsilon'' - \mu''\epsilon')^2}} \quad (5)$$

$$Z = \sqrt{\sqrt{(\mu''^2 + \mu'^2)} / \sqrt{(\epsilon''^2 + \epsilon'^2)}} \quad (6)$$

Where f and c are the frequency of the electromagnetic wave and the velocity of light, respectively.

Supplementary tables

Supplementary Table S1: MA performance of best MA materials reported in open literatures

| Samples in matrices | wt % | Max RL [dB] | Thickness [mm] (RL ≤ -10 dB) | Testing frequency range [GHz] | Frequency range [GHz] (RL ≤ -10 dB) | Refs |
|---|--------|---------------|------------------------------|-------------------------------|-------------------------------------|-----------|
| Air@rGO@Fe ₃ O ₄ microsphere in wax | 33 | -52.0 | 2.8 | 1-18 | 7.5-14.7 | This work |
| acid treated Air@rGO@Fe ₃ O ₄ microsphere in wax | 33 | -46.0 | 3.5 | 1-18 | 6.3-12.3 | This work |
| Flower-like CuS hollow microspheres in wax | 30 | -31.5 | 1.8 | 1-18 | 14.4-18.0 | [2] |
| Silica–nickel–carbon microspheres in wax | 40 | -37.6 | 2.4 | 2-18 | 12.0-18.0 | [12] |
| Hollow CdSe in wax | 70 | -31.0 | 2.0 | 2-18 | 4.0-7.0, 17.0-18.0 | [13] |
| RGO–CoFe ₂ O ₄ /GNSs in cyanate ester resin | 13 | -21.8 | 1.2 | 8-13 | 9.6-12.4 | [14] |
| core–shell carbon–magnetite porous nanorods in wax | 30vol% | -60.0 | 2.6 | 2-18 | 5.1-10.1 | [15] |
| RGO/flake carbonyl iron po/polyaniline in wax | 70 | -38.8 | 2.0 | 2-18 | 6.5-7.5, 11.0-12.0 | [16] |
| graphene@Fe ₃ O ₄ @SiO ₂ @PA NI in wax | 25 | -40.7 | 2.5 | 2-18 | 10.5-16.3 | [17] |
| graphene@Fe ₃ O ₄ @C@PANI in wax | 25 | -44.2 | 3.0 | 2-18 | 9.7-15.5 | [18] |
| SWCNT/CoFe ₂ O ₄ nanocomposites in wax | 50 | -30.7 | 2.0 | 2-18 | 9.3-16.5 | [19] |
| graphene@Fe ₃ O ₄ @carbon@MnO ₂ in wax | 25 | -38.8 | 1.8 | 2-18 | 12.3-17.7 | [20] |
| CoFe ₂ O ₄ hollow sphere/graphene in wax | 60 | -18.5 | 2.0 | 1-18 | 11.5-15.2 | [21] |
| reduced graphene oxide-CoFe ₂ O ₄ in wax | 50 | -44.1 | 1.6 | 2-18 | 13.3-18.0 | [22] |
| Co-doped MnO ₂ in wax | 20 | -17.5 | 2.0 | 2-18 | 10.96-16.13 | [23] |
| CoxFe _{3-x} O ₄ (x=0-1) spheres in wax | 75 | -41.1 | 2.0 | 2-18 | 10.0-14.2 | [24] |
| NiCoP/RGO in wax | 75 | -17.8 | 1.5 | 2-18 | 6.2-9.3 | [25] |
| Fe ₃ O ₄ /graphene capsules in wax | 30 | -32.0 | 3.5 | 2-18 | 7.3-11.5 | [26] |
| RGO-PPy-Co ₃ O ₄ in wax | 50 | -43.5 | 3.2 | 2-18 | 8.9 - 15.3 | [27] |

| | | | | | | |
|---|----|-------|-----|--------|-------------|------|
| CuS on magnetically decorated graphene in wax | 20 | -54.5 | 2.5 | 2-18 | 9.2-13.7 | [28] |
| hierarchical NiCo ₂ O ₄ in wax | 50 | -25.5 | 4.0 | 1-18 | 3.7-5.5 | [29] |
| α-Co/graphene in wax | 60 | -47.5 | 2.0 | 1-18 | 9.7-13.6 | [30] |
| Fe ₃ O ₄ @SiO ₂ @RGO in wax | 20 | -26.6 | 3.0 | 2-18 | 7.7-11.3 | [31] |
| ring-shaped FeCo@ carbon fiber in wax | 20 | -37.7 | 1.8 | 2-18 | 8.2-10.1 | [32] |
| cobalt/polypyrrole in wax | 30 | -33.0 | 2.0 | 1-18 | 11.7-16.47 | [33] |
| cobalt–cobalt oxide in wax | 60 | -30.5 | 1.7 | 2-18 | 12.6-17.3 | [34] |
| Twin carbon nanocoils in wax | 15 | -36.1 | 2.0 | 2-18 | 14.0-18.0 | [35] |
| Co/carbon nanotube-graphene in wax | 30 | -65.6 | 2.2 | 2-18 | 10.0-13.5 | [36] |
| rugby-shaped CoFe ₂ O ₄ in wax | 50 | -34.1 | 2.5 | 1-18 | 12.3 - 14.9 | [37] |
| Co/PVDF | 25 | -38.9 | 2.5 | 2-18 | 5.5-8.3 | [38] |
| Fe ₃ O ₄ @ZnO in wax | 50 | -22.7 | 3.5 | 2-18 | 10.08-15.97 | [39] |
| hollow porous Ni/SnO ₂ in wax | 50 | -36.7 | 1.7 | 1-18 | 10.6-14.0 | [40] |
| hollow urchinlike α-MnO ₂ in wax | 50 | -41.0 | 1.9 | 0.1-18 | 7.5-10.0 | [41] |
| BaTiO ₃ nanotubes in wax | 70 | -21.8 | 2.0 | 0.5-15 | 13.2-15 | [42] |
| RGO/CoFe ₂ O ₄ in wax | 50 | -42.2 | 2.3 | 2-18 | 11.8-17.0 | [43] |
| mesoporous carbon in wax | 60 | -27.1 | 2.2 | 2-18 | 12.5-18.0 | [44] |
| Co doped mesoporous carbon composites in wax | 30 | -41.9 | 1.8 | 2-18 | 11.4 -15.8 | [45] |
| Ag@Fe ₃ O ₄ /RGO in wax | 50 | -40.1 | 2.0 | 2-18 | 9.4 - 12.5 | [46] |
| graphene@Fe ₃ O ₄ @carbon in wax | 25 | -30.1 | 1.8 | 2-18 | 12.1- 17.5 | [47] |
| Thermally reduced graphene networks in wax | 1 | -43.5 | 3.5 | 2-18 | 9.36-16.83 | [48] |
| Ni _{0.6} Zn _{0.4} Fe ₂ O ₄ /PANI in wax | 70 | -41.0 | 2.6 | 2-18 | 10.3-15.3 | [49] |
| Ni _{0.5} Zn _{0.5} Fe ₂ O ₄ ferrite nanofiber in wax | 15 | -14.1 | 3.6 | 2-18 | 8.1-12.5 | [50] |
| carbon–silica/FeNi in wax | 40 | -45.6 | 3.0 | 0.5-18 | 9.1-14.3 | [51] |
| Fe–Co/NPC in wax | 50 | -21.7 | 1.2 | 2-18 | 12.2-18.0 | [52] |

Supplementary references

- Y. J. Chen, G. Xiao, T. S. Wang, Q. Y. Yang, L. H. Qi, Y. Ma, P. Gao, C. L. Zhu, M. S. Cao and H. B. Jin, *J.Phys.Chem.C*, 2011, **115**, 13603-13608.
- B. Zhao, G. Shao, B. B. Fan, W. Y. Zhao, Y. J. Xie and R. Zhang, *J. Mater. Chem. A*, 2015, **3**, 10345-10352.
- G. X. Tong, Y. Liu, T. T. Cui, Y. N. Li, Y.T. Zhao and J. G. Guan, *Appl. Phys. Lett.*, 2016, **108**, 072905.
- P. Liu, P. H. Zhou, J. L. Xie and L. J. Deng, *J. Appl. Phys.*, 2012, **111**, 093905.
- Y. P. Duan, Z. Liu, H. Jing, Y. H. Zhang and S. Q. Li, *J. Mater. Chem.*, 2012, **22**, 18291-18299.
- H. L. Yu, T. S. Wang, B. Wen, M. M. Lu, X. Zheng, C. L. Zhu, Y. J. Chen, X. Y. Xue, C. W. Sun and M. S. Cao, *J.*

- Mater. Chem.*, 2012, **22**, 21679-21685.
7. C. Kittel, *Phys. Rev.*, 1948, **73**, 155-161.
8. G. X. Tong, W. H. Wu, J. G. Guan, H. S. Qian, J. H. Yuan and W. Li, *J. Alloys Compd.*, 2011, **509**, 4320-4326.
9. S. B. Ni, X. L. Sun, X. H. Wang, G. Zhou, F. Yang, J. M. Wang and D. Y. He, *Mater. Chem. Phys.*, 2010, **124**, 353-358.
10. H. L. Lv, G. B. Ji, H. Q. Zhang, M. Li, Z. Z. Zuo, Y. Zhao, B. S. Zhang, D. M. Tang and Y. W. Du, *Sci. Rep.*, 2015, **5**, 18249.
11. H. L. Lv, G. B. Ji, X. H. Liang, H. Q. Zhang and Y. W. Du, *J. Mater. Chem. C*, 2015, **3**, 5056-5064.
12. Z. G. An and J. G. Zhang, *Dalton Trans.*, 2016, **45**, 2881-2887.
13. M. H. Cao, H. Q. Lian and C. W. Hu, *Nanoscale*, 2010, **2**, 2619-2623.
14. F. Ren, G. M. Zhu, P. G. Ren, K. Wang, X. P. Cui and X. G. Yan, *Appl. Surf. Sci.*, 2015, **351**, 40-47.
15. M. Jazirehpour and S. A. S. Ebrahimi, *J. Alloys Compd.*, 2015, **639**, 280-288.
16. Y. Xu, J. H. Luo, W. Yao, J. G. Xu and T. Li, *J. Alloys Compd.*, 2015, **636**, 310-316.
17. L. Wang, J. F. Zhu, H. B. Yang, F. Wang, Y. Qin, T. Zhao and P. Zhang, *J. Alloys Compd.*, 2015, **634**, 232-238.
18. L. Wang, Y. Huang, C. Li, J. J. Chen and X. Sun, *Compos. Sci. Technol.*, 2015, **108**, 1-8.
19. G. Li, L. M. Sheng, L. M. Yu, K. An, W. Ren and X. L. Zhao, *Mater. Sci. Eng. B*, 2015, **193**, 153-159.
20. L. Wang, Y. Huang, C. Li, J. J. Chen and X. Sun, *Phys. Chem. Chem. Phys.*, 2015, **17**, 5878-5886.
21. M. Fu, Q. Z. Jiao, Y. Zhao and H. S. Li, *J. Mater. Chem. A*, 2014, **2**, 735-744.
22. M. Zong, Y. Huang and N. Zhang, *Appl. Surf. Sci.*, 2015, **345**, 272-278.
23. Y. P. Duan, Z. Liu, H. Jing, Y. H. Zhang and S. Q. Li, *J. Mater. Chem.*, 2012, **22**, 18291-18299.
24. R. L. Ji, C. B. Cao, Z. Chen, H. Z. Zhai and J. Bai, *J. Mater. Chem. C*, 2014, **2**, 5944-5953.
25. W. C. Ye, J. J. Fu, Q. Wang, C. M. Wang and D. S. Xue, *J. Magn. Magn. Mater.*, 2015, **395**, 147-151.
26. X. Jian, B. Wu, Y. F. Wei, S. X. Dou, X. L. Wang, W. D. He and N. Mahmood, *ACS Appl. Mater. Interfaces*, 2016, **8**, 6101-6109.
27. P. Liu and Y. Huang, *Rsc Adv.*, 2013, **3**, 19033-19039.
28. P. B. Liu, Y. Huang, J. Yan, Y. W. Yang and Y. Zhao, *ACS Appl. Mater. Interfaces*, 2016, **8**, 5536-5546.
29. M. Zhou, F. Lu, T. Y. Lv, X. Yang, W. W. Xia, X. S. Shen, H. Hui and X. G. Zeng, *J. Phys. D: Appl. Phys.*, 2015, **48**, 215305.
30. G. H. Pan, J. Zhu, S. L. Ma, G. B. Sun and X. J. Yang, *ACS Appl. Mater. Interfaces*, 2013, **5**, 12716-12724.
31. Y. F. Pan, G. S. Wang and Y. H. Yue, *Rsc Adv.*, 2015, **5**, 71718-71723.
32. Y. Z. Wan, J. Xiao, C. Z. Li, G. Y. Xiong, R. S. Guo, L. L. Li, M. Han and H. L. Luo, *J. Magn. Magn. Mater.*, 2016, **399**, 252-259.
33. H. C. Wang, N. Ma, Z. R. Yan, L. Deng, J. He, Y. L. Hou, Y. Jiang and G. G. Yu, *Nanoscale*, 2015, **7**, 7189-7196.
34. Z. Z. Wang, H. Bi, P. H. Wang, M. Wang, Z. W. Liu, L. Shen and X. S. Liu, *Phys. Chem. Chem. Phys.*, 2015, **17**, 3796-3801.
35. N. J. Tang, W. Zhong, C. Au, Y. Yang, M. G. Han, K. J. Lin and Y. W. Du, *J. Phys. Chem. C*, 2008, **112**, 19316-19323.
36. X. S. Qi, Q. Hu, J. L. Xu, R. Xie, Y. Jiang, W. Zhong and Y. W. Du, *Rsc Adv.*, 2016, **6**, 11382-11387.
37. S. L. Zhang, Q. Z. Jiao, Y. Zhao, H. S. Li and Q. Wu, *J. Mater. Chem. A*, 2014, **2**, 18033-18039.
38. X. J. Zhang, G. C. Lv, G. S. Wang, T. Y. Bai, J. K. Qu, X. F. Liu and P. G. Yin, *Rsc Adv.*, 2015, **5**, 55468-55473.
39. Z. J. Wang, L. N. Wu, J. G. Zhou, B. Z. Shen and Z. H. Jiang, *Rsc Adv.*, 2013, **3**, 3309-3315.
40. B. Zhao, W. Y. Zhao, G. Shao, B. B. Fan and R. Zhang, *Dalton Trans.*, 2015, **44**, 15984-15993.
41. M. Zhou, X. Zhang, J. M. Wei, S. L. Zhao, L. Wang and B. X. Feng, *J. Phys. Chem. C*, 2011, **115**, 1398-1402.
42. Y. F. Zhu, L. Zhang, T. Natsuki, Y. Q. Fu and Q. Q. Ni, *ACS Appl. Mater. Interfaces*, 2012, **4**, 2101-2106.

43. M. Zong, Y. Huang, N. Zhang and H. W. Wu, *J. Alloys Compd.*, 2015, **644**, 491-501.
44. Y. C. Du, T. Liu, B. Yu, H. B. Gao, P. Xu, J. Y. Wang, X. H. Wang and X. J. Han, *Mater. Chem. Phys.*, 2012, **135**, 884-891.
45. Q. Lian, L. D. Wang, H. J. Wu and H. Wu, *Nano*, 2014, **9**, 1450033.
46. G. Z. Liu, W. Jiang, Y. P. Wang, S. T. Zhong, D. P. Sun, J. Liu and F. S. Li, *Ceram. Int. (Part B)*, 2015, **41**, 4982-4988.
47. Y. Huang, L. Wang and X. Sun, *Mater. Lett.*, 2015, **144**, 26-29.
48. W. W. Liu, H. Li, Q. P. Zeng, H. N. Duan, Y. P. Guo, X. F. Liu, C. Y. Sun and H. Z. Liu, *J. Mater. Chem. A*, 2015, **3**, 3739-3747.
49. M. Wang, G. B. Ji, B. S. Zhang, D. M. Tang, Y. Yang and Y. W. Du, *J. Magn. Magn. Mater.*, 2015, **377**, 52-58.
50. X. G. Huang, J. Zhang, M. Lai and T. Y. Sang, *J. Alloys Compd.*, 2015, **627**, 367-373.
51. G. X. Li, Y. X. Guo, X. Sun, T. Wang, J. H. Zhou and J. P. He, *J. Phys. Chem. Solids*, 2012, **73**, 1268-1273.
52. X. M. Zhang, G. B. Ji, W. Liu, B. Quan, X. H. Liang, C. M. Shang, Y. Cheng and Y. W. Du, *Nanoscale*, 2015, **7**, 12932-12942.